Indian J. Phys. 77B (1), 49-62 (2003)

AN INTERNATIONAL JOURNAL
IJP

Femtosecond time–resolved coherent Raman spectroscopy for probing molecular dynamics

M Schmitt, T Siebert and W Kiefer*

Institut für Physikalische Chemie der Universität Würzburg, Am Hubland, D-97074 Würzburg, Federal Republic of Germany

e-mail : wolfgang.kiefer@mail.uni-wuerzburg.de

Abstract This paper reviews results on wavepacket dynamics investigated by means of femtosecond time–resolved four–wave–mixing (FWM) spectroscopy. First, it is shown that by making use of the various degrees of freedom which are offered by these nonlinear Raman or transient grating techniques information about molecular dynamics on different potential energy surfaces can be accessed and separated from each other. By varying the timing and wavelengths of the laser pulses as well as the wavelength of the detection window for the FWM signal, different dynamics are coherently excited and probed by the nonlinear spectroscopy. As a model system iodine in the gas phase was used. Second we report about selective excitation of ground vibrational modes in the electronic ground state of porphyrin systems by means of a femtosecond time-resolved CARS (coherent anti-Stokes Raman scattering) scheme. By detecting the spectrum of the transient CARS signal, a detailed mapping of the dynamics initiated by the stimulated Raman pump process is achieved. The method is able to yield the dephasing behaviour and spectral information of the investigated system at the same time. The different contributions to the ground state vibrational dynamics are selected by changing the direction of the CARS signal analyzer in the polarization arrangement used.

Keywords Femtosecond time-resolved Raman spectroscopy, four-wave mixing, CARS signal, molecular dynamics

PACS Nos. 06.60.Jn, 42.65.Dr, 42.65.Hw

Introduction

Since the discovery of the Raman effect [1] in 1928 many special techniques, and myriads of applications for Raman spectroscopy were developed. Of particular interest has been the inelastic, nonlinear scattering in which the vibrational degrees of freedom in molecular systems are measured using Raman methodologies. Since the first observation of coherent Raman scattering via the mixing of four electromagnetic waves in 1965, several other nonlinear Raman phenomena have been observed and developed as spectroscopic methods. These coherent Raman spectroscopies, especially those involving four-wave mixing (FWM) phenomena have been widely used for numerous applications in condensed– and gas–phase analysis, plasma diagnostics, investigations of molecular relaxation processes, temperature and concentration measurements, condensed phase studies, and, very recently in femtochemistry. Similar to frequency tunable sources of coherent radiation, which revolutionized nonlinear optics in its early days, allowing many sophisticated spectroscopic experiments including nonlinear spectroscopic studies, to be performed, the impressive progress of femtosecond laser in the 1990s has resulted in the breakthrough of non-linear Raman spectroscopy to new unexplored areas, giving rise to several elegant new ideas and approaches, permitting more complicated systems and problems to be studied, and leading to the measurements of fundamental importance.

The high intensity achieved by femtosecond lasers favors the application of nonlinear methods like four–wave mixing (FWM) spectroscopies for the study of ultrafast intramolecular dynamical processes. Since Leonhardt *et al.* [3] applied femtosecond laser pulses to the observation of time–resolved coherent anti–Stokes Raman scattering (CARS), several groups have reported sub–picosecond and femtosecond time–resolved CARS measurements [4–13]. Theories for these time–resolved nonlinear spectroscopical methods were developed by several researchers [7, 14–17]. Time–resolved coherent Raman scattering techniques have been widely employed in condensed phase studies of vibrational dephasing [3, 4, 8, 18–26]. However, these methods have not been exploited on the subpicosecond time

*Corresponding Author

scale for gas phase studies until recently Hayden and Chandler [13] reported the application of femtosecond time-resolved coherent Raman techniques to excite and monitor the evolution of vibrational coherence in gas phase samples of benzene as well as 1,3,5-hexatriene. Recently, nonlinear four-wave mixing (FWM) techniques were incorporated in different temporal pulse schemes to extract the dynamics of atomic, unimolecular, and bimolecular systems in the gas phase by Zewail and co-workers [27]. For the FWM a three dimensional forward geometry (folded BOXCARS arrangement) [28-30] was chosen Degenerate FWM (DFWM) as well as a two-color grating experiment [31] were used to replace the probe pulse in a pump-probe scheme. Also the FWM process itself was used to gain information on the decay dynamics of atomic Na.

More recently, fs-CARS has been extended in our group to the study of molecular systems in the gas phase, where it has proven to be a valuable tool in the excitation and probing of coherent nuclear motion in the electronic ground as well as excited state in simple molecular systems [32-42].

In the present paper we review the work on femtosecond time-resolved FWM spectroscopy performed in our laboratories recently. We would like to point out the main advantages of this technique and to emphasize its capability for investigating ground state dynamics. We have demonstrated that by the CARS method one can observe the dynamics of a wavepacket either evolving on the ground or an excited state potential energy surface (PES) [32]. The dynamics which shows itself in the CARS transient depends on the relative timing of the three laser pulses giving rise to the nonlinear FWM process. Next to the timing of the laser pulses there are other degrees of freedom which can be varied in order to gain even more information on the ultrafast ro-vibrational dynamics evolving in the excited molecules. The following points will be discussed below: (i) we will demonstrate that the timing of the laser pulses can be used to obtain information about dynamics evolving on different PESs of iodine molecules; (ii) the laser wavelengths which determine the electronic as well as rovibrational resonances and through this the preparation of the wavepackets on the PES of the molecules also determine which FWM process takes place (CARS, or CSRS, which is the Stokes analogue to CARS —coherent Stokes Raman scattering and DFWM = degernerate four-wave mixing); (iii) the wavelength window which is opened for the detection of the FWM signal detects different dynamical information contained in the transients; (iv) we demonstrate that also for more complex molecules (porphyrins) mode dynamics are accessible making use of the spectral components of the transient FWM signal [43-45]. We show that even a controlled selective excitation of modes on the femtosecond time scale can be performed.

2. Theory and methodology

In the following, the formalism necessary for the description of third order optical interactions in the form of coherent Raman techniques and transient grating, is presented in a time-resolved scenario using third order perturbation theory in the weak field limit.

We consider the interaction of three pulsed laser fields k_1, k_2 and k_3 denoted by their respective wave vectors with an electronic two state system, namely the ground state $|g\rangle$ and an excited state $|e\rangle$. The frequencies of the fields are resonant with the $|g\rangle \leftrightarrow |e\rangle$ electronic transition so that the interaction with the ultrashort pulses prepares nuclear wavepackets within the two states. Since the spectral bandwidth of the femtosecond laser pulses employed in the experiments described in this work can be characterized with a FWHM of approximately 200-250 cm^{-1}, the coherent superposition of multiple vibrational states within an electronic state is possible. The phase coupled excitation of vibrational states to a nuclear wavepacket allows for the vibrational dynamics taking place within the excited molecular system to be observed via their influence on the transient FWM-signal. [34, 35] The mechanism with which vibrational wavepackets manifest themselves in the transient FWM-signal will be shown in the next section.

Two pulses k_1, k_2 are fired simultaneously while a third pulse k_3 is time delayed with respect to the time coincident pulse pair. The fields induce a time dependent polarization which can be written as:

$$P(t) = \langle \psi(t) | \mu | \psi(t) \rangle$$

where $\psi(t)$ is the wavefunction of the system μ is the dipole moment and the bra-kets denote integration over the molecular coordinates.

Due to energy conservation : $\omega_{FWM} = \omega_1 - \omega_2 + \omega_3$ has to be fulfilled. Additionally, due to the phase matching condition $k_{FWM} = k_1 - k_2 + k_3$ also has to be fulfilled and the k vectors of the lasers and the signal must not be arranged arbitrarily. In the experiments presented here the socalled folded BOXCARS arrangement, which allows for a spatial separation of all laser beams and the signal has been chosen [30]. The polarization emitted in direction $k_1 - k_2 + k_3$ is detected so that of all components of $P(t)$ we need to consider the third-order terms $P^{(3)}(t, k_1 - k_2 + k_3)$ only. The experimental signal is obtained via time integrating over a finite interval T_e and explicitly depends on the delay time Δt between the time coincident pulse pair k_1 and k_2 and k_3. Detection of the emitted radiation yields the signal

$$S(\Delta t) = \int_{-\infty}^{T_2} dt \left| P^{(3)}(t) \right| \qquad (2)$$

where we have noted the dependence on the delay time Δt explicitly.

The time-delay between the simultaneously acting pulses k_1, k_2 and the third pulse k_3 might be either positive (k_1, k_2 before k_3) or negative (k_1, k_2 after k_3).

For non-overlapping pulses and positive delay times the pulses with k_1 and k_2 prepare a wavepacket $|g^{(2)}(-k_2+k_2)\rangle$ in the ground state. The time delayed third pulse then prepares the first order state $|e^{(1)}(k_3)\rangle$ i in the excited state $|e\rangle$. The scalar product of these states contributes to the third order polarization. There is a second and third contribution to $P^{(3)}(t)$ which correlates the unperturbed ground state wavefunction j $|g^{(0)}\rangle$ with the third order state $|e^{(3)}(k_2+k_2+k_3)\rangle$ and the second order wavefunction $|g^{(2)}(-k_2+k_3)\rangle$ with the first order state $e^{(1)}(k_1)\rangle$, respectively so that the polarization is given as the sum:

$$P^{(3)}(\Delta t, k_1-k_2+k_3)=\left\{\left\langle g^{(2)}(k_2-k_1)|\mu|e^{(1)}(k_3)\right\rangle\right. \quad (3)$$

$$\left.+\left\langle g^{0}|\mu|e^{(3)}(k_1-k_2+k_3)\right\rangle+\left\langle g^{(2)}(k_2-k_3)|\mu|e^{(1)}(k_1)\right\rangle\right\}+cc.$$

Note that if the arguments k_j (j = 1; 2; 3) appear in the bra-vectors, their corresponding signs are changed compared with the ket-states, so that the phase matching condition $k_{FWM}=k_1-k_2+k_3$ is fulfilled. As discussed above the first term of equation (3) reflects ground state motion. The third order wavefunction in the excited state $e^{(3)}(k_1-k_2+k_3)\rangle$ of the second term in equation (3) is prepared in a first step via the simultaneous acting pulses k_1 and k_2 which yields a ground state wavepacket $g^{(2)}(k_1-k_2)\rangle$ which afterwards evolves in time. The one photon probe process by the pulse k_3 which originates from this initial state results in a third order wavefunction in $|e>$ which is projected on $|g^{(0)}\rangle$. As a consequence the second term in equation (3) also reflects the dynamics of the ground state $|g>$ On the other hand the third term contains an excited state wavepacket (which actually has two components corresponding to excitation with k_1 and k_2). This wavepacket then serves as initial state for the stimulated emission process down to the ground state.

For negative delaytimes a single pulse k_3 prepares a wavepacket $e^{(1)}(k_3)>$ in the upper excited electronic state which is probed by the time-delayed combination of pulses k_1 and k_2. There we find the third-order polarization to be of the form:

$$P^{(3)}(\Delta t, k_1-k_2+k_3)=\left\{\left\langle g^{(2)}(k_2-k_1)|\mu|e^{(1)}(k_3)\right\rangle\right.$$

$$\left.+\left\langle g^{0}|\mu|e^{(3)}(k_1-k_2+k_3)\right\rangle\right\}+cc., \quad (4)$$

where μ is the projection of the transition dipole moment for the $|g\rangle \leftrightarrow |e\rangle$ transition on the electric field vector.

The single contributions of $P^{(3)}$ for positive and negative delay times differ with respect to absorption and emission processes induced by the different pulses.

The FWM techniques applied to the investigation of molecular dynamics throughout this work were the coherent Raman techniques CARS (coherent anti-Stokes Raman scattering) and CSRS (coherent Stokes Raman scattering) and the degenerate four-wave mixing spectroscopy (DFWM). One signal transforms into the other by changing the frequencies (ω_1, ω_2, $\omega_3=\omega_1$) (CARS for $\omega_1>\omega_2$ or CSRS for $\omega_1<\omega_2$) into ($\omega_1=\omega_2=\omega_3$) (DFWM). The molecular states prepared, propagated and interrogated by introducing different scenarios of variable time delays and color schemes (CARS, CSRS and DFWM) between the laser pulses involved in these forms of FWM will be discussed in the results and discussion chapter.

3. Experimental

The setup used for the femtosecond FWM experiments is shown in Figure 1 and is described in the following. The laser system is based on a Ti:Sapphire oscillator (Coherent MIRA) pumped by the multiline output of an Ar^+ ion laser (Coherent Innova 310) running at about 8 W. The pulses were produced by the oscillator at a repetition rate of 83 MHz having temporal pulse widths of about 100 fs. The pulse energy was less than 10 nJ and the pulses were centered at about 800 nm having a spectral width (FWHM) of 14 nm. For the amplification of the pulses a regenerative Ti:Sapphire amplifier system (Clark-MXR) was used. The pulses were stretched to a duration of > 200 ps before amplification. The regenerative Ti:Sapphire amplifier was pumped by a frequency doubled Nd:YAG laser at a repetition rate of 1 kHz. After recompression the pulses had energies of about 1.5 mJ and temporal widths of less than 100 fs.

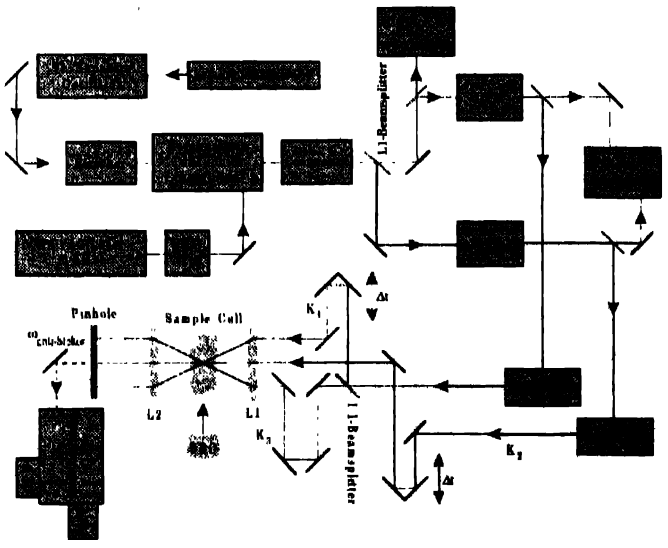

Figure 1. Experimental setup showing the femtosecond laser system and the beam path of the time-resolved BOXCARS arrangement. Computer controlled actuators are used to vary the relative arrival time of the femtosecond pulses at the sample. The monochromator is equipped with both photomultiplier tube (PMT) and CCD camera.

In order to have two different colors available, the 800 nm pulse train was split into two parts by means of a beam splitter.

Using two four-path OPAs (optical parametric amplifiers, Light Conversion) two independent wavelengths could be chosen. The laser pulses were produced using sum frequency generation between signal and idler output of the OPA as well as second harmonic generation of either the signal or the idler light. The pulses were finally compressed in double-pass two-prism arrangements resulting in temporal pulse widths of about 70 fs (assuming Gaussian pulse profiles).

One of the OPA outputs was branched by a 1:1 beam splitter to produce the two pulses k_1 and k_2. These two beams were then aligned parallel to one another and spatially overlapped at the common focus in the sample cell by the achromatic lens L1. The third beam k_3 (output of the second OPA) was aligned parallel to and spatially separated from the two pulses k_1 and k_2 and passed through the top of lens L1, focussing in the same region as the two pump beams. This folded BOXCARS configuration was employed in order to seperate the signal from the incoming pump and probe beams [30]. In this geometry the phase-matching condition is fulfilled.

The pulses could be delayed in time relative to each other by means of Michelson interferometer arrangements. In the experiments presented in this paper, the pulses k_1 and k_2 were kept temporally overlapped and fixed. The FWM transients were recorded as a function of delay time Δt between the pulse k_3 and the two fixed and time coincident pulses k_1 and k_2. The relative timing between the different pulses was varied with a computer-controlled actuator that allowed for optical delay up to 3 ns with a minimal step size of 6 fs. The determination of the position of temporal overlap (time zero) between the different beam pairs was made using a cross correlation setup with second harmonic generation as well as sum frequency mixing in a thin, phase-matched BBO crystal.

The fs FWM signal pulse generated in the sample travels in a direction determined by the phase- matching condition. As this direction is different from that of the incident laser beams the signal can easily be separated by a spatial filter. The FWM beam was collimated by a second achromatic lens L2. In order to remove the stray laser light and to spectrally analyze the signal a monochromator (Acton SpectraPro-500) is used. The detection is performed in two ways: (i) a fast photomultiplier tube (RCA C31024 A) measures the light leaving the monochromator. The signal-to-noise ratio is enhanced by means of a boxcar integrator (EG&G model 4121B) in gated-integrator mode, as well as by numerical averaging of several pulses. The latter is also used to smooth the multichannel output of (ii) a CCD camera (Photometrics) which is attached to the monochromator without exit slit. The broadband detection offers many advantages as the whole spectral range of the FWM signal can be resolved for each pulse.

In this review, we present results on femtosecond investigations of iodine in the gas phase as well as on porphyrin solutions. The gas phase iodine sample was kept in a quartz cell and heated to $\approx$ 80°C in order to increase the vapor pressure. For this temperature, the vapor pressure of iodine was $\approx$ 2 kPa. The investigated porphyrin samples have been used as purchased (Porphyrin Products). All measurements have been performed on solutions, using a flow-type cuvette built from a rectangular glass capillary (Vitro Dynamics Inc.). As solvent we chose dichloromethane, because it possesses only weak vibrational bands in the excitation region and is relatively inert and non-polar compared with other solvents. Sample concentrations have been adjusted to yield a linear absorption of typically 1.2 OD for the strongest Q-band in a 1 mm path-length cuvette.

4. Results and discussion

Here, we demonstrate the main advantages of femtosecond time-resolved FWM spectroscopy by discussing some of the experimental results on different molecules obtained in our laboratories. We present results which give a flavor of the wide capabilities of the FWM techniques. First, for iodine in the gas phase, we show that by just varying the wavelengths and/or timing of the laser pulses selectively different dynamics can be accessed. Second, we demonstrate that by using the excitation scheme of the nonlinear Raman spectroscopy also a controlled mode excitation in the ground state of complex molecular systems is possible. As example we used the excitation of vibrational modes of porphyrins.

4.1 Femtosecond time-resolved four-wave mixing spectroscopy in gaseous iodine :

The DFWM transient discussed in the following was recorded using three laser fields having the same central wavelength λ_0, which is resonant with discrete ro-vib eigenstates in the excited B state of iodine. While two laser pulses (k_1 and k_2 coincident in time the third pulse (k_3) arrives with a variable time delay. Figure 2(A) shows a typical DFWM transient of iodine as a function of the delay time Δt between the variable laser pulse, k_3, and the fixed, simultaneous laser pulses k_1 and k_2. The transient exhibits well defined 300 fs beats, corresponding to a vibrational energy spacing of about 111 cm^{-1}. This agrees well with the experimental vibrational energy spacings in the excited B state of gaseous iodine accessed by the 620 nm lasers around $v' \approx 7$. For positive delay times ($\Delta t > 0$) additional beats having about twice this wavenumber appear. These oscillations show a period of 155 fs, which corresponds to an energy spacing of 215 cm^{-1} and reflects the dynamics of a wavepacket within the electronic ground state of iodine around $v'' \approx 7$. The Fast Fourier Transform (FFT) spectrum (not shown in this paper) also confirms the above mentioned interpretation.

In the fs-CARS experiment two laser pulses (k_1 and k_3) which are referred to as *pump*-lasers have the same wavelength $\lambda_1 = \lambda_3$. The third laser pulse (k_2) referred to as *Stokes*-laser is tuned to a lower wavelength λ_2 in such a way that the difference between λ_1 and λ_2 is resonant with a vibratio

Raman transition in the iodine molecule in the ground state. Figure 2(B) shows the experimentally observed CARS intensity as a function of delay time Δt between the pump pulse k_3 and the two time coincident pulses λ_1 and λ_2 for I_2 vapour. The transient was obtained for a pump wavelength $\lambda_1 = \lambda_2 = 620$ nm and a Stokes wavelength $\lambda_3 = 645$ nm detecting the coherent anti-Stokes signal (aS) at $\lambda_{aS} = 596$ nm with the PMT tube. For negative delay times ($\Delta t < 0$) of k_3, the transient is characterized by beats with a period of approximately 300 fs, which corresponds to an energy difference of 111 cm^{-1}. This value agrees with the energy spacing found between the vibrational eigenstates of iodine in the excited B state, which are reached by the $\lambda_3 = 620$ nm laser pulse from the ground state. For positive delay times ($\Delta t > 0$) the signal shows oscillations at about twice the frequency of the oscillations at negative delay times ($\Delta t < 0$). These short time oscillations for $\Delta t > 0$ show a period of 160 fs, corresponding to the wavepacket motion prepared by coherent two photon pumping (k_1 and k_2) around the third vibrational level in the ground X state of iodine, because the wavelength difference between k_1 and k_2 laser was tuned to the second overtone ($\Delta v'' = 3$) of the I_2 ground state vibration. The average period of the oscillations corresponds to a vibrational wavenumber spacing of about 208 cm^{-1}. This agrees with the vibrational energy spacing in the ground X state of iodine around $v'' = 3$ as observed from continuum resonance Raman experiments [46].

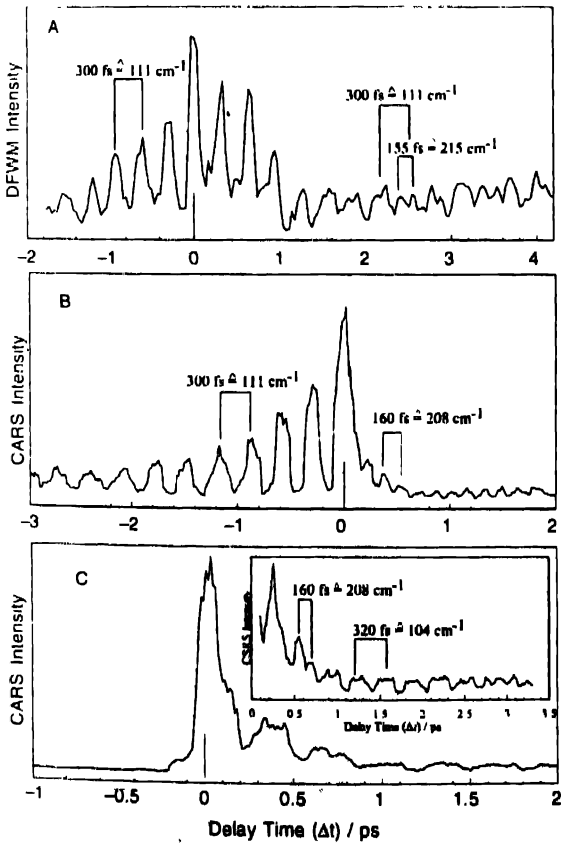

ure 2. Femtosecond FWM transients of gaseous iodine: (A) fs–DFWM sient ($\lambda_n = 620$ nm). (B) fs–CARS transient ($\lambda_1 = \lambda_3 = 620$ nm, λ_2 45 nm, $\lambda_{aS} = 596$ nm). (C) fs–CSRS transient ($\lambda_1 = \lambda_3 = 615$ nm, λ_2 nm, $\lambda_3 = 641$ nm).

The fs–CSRS transient displayed in Figure 2(C) shows a completely different time behaviour than the DFWM [see Figure 3(A)] or the CARS [see Figure 2(B)] transient. In the fs–CSRS experiment also three laser fields interact with the ensemble of I2 molecules. Two laser pulses (k_1 and k_3) have the same wavelengths, $\lambda_1 = \lambda_3$, and furtheron will be referred to, in consistency with the CARS experiment, as pump lasers. The third laser (k_2) (anti–Stokes) is tuned, in contrast to the CARS experiment, to a lower wavelength, λ_2, such that the difference between pump and anti–Stokes laser wavelength is resonant with a vibrational transition in the ground state. Figure 2(C) shows a fs–CSRS transient for gaseous iodine as a function of the delay time Δt between the pulse k_3 and the two time coincident pulses k_1 and k_2. For a pump wavelength $\lambda_1 = \lambda_3 = 615$ nm and an anti–Stokes wavelength $\lambda_3 = 591$ nm the coherent Stokes signal is detected by means of a PMT tube at $\lambda_S = 641$ nm. As in the case for the CARS transient also here the wavelengths of the pump lasers k_1 and k_3 determine where the interaction with the excited state potential takes place. The difference of the wavelengths between pump (k_1) and anti–Stokes (k_3) laser ($\lambda_3 - \lambda_1$), which was chosen to be resonant with the second overtone $\Delta v'' = 3$ within the ground state of the iodine molecules, gives the position accessed in the ground state potential. The transient shows neither a signal nor a beating structure for negative delay times ($\Delta t < 0$). For positive delay times ($\Delta t > 0$) the transient exhibits well defined 320 fs beats, corresponding to a vibrational energy spacing of about 104 cm^{-1}. This agrees well with the experimental vibrational energy spacings in the excited B state of gaseous iodine accessed by the 615 nm pump lasers around $v' \approx 7$. Also beats having about twice this wavenumber appear. These can be assigned to the electronic ground state. The FFT spectrum of the CSRS transient (not shown here) also exhibits two distinct components at 111 and 208 cm^{-1}. The peak at 111 cm^{-1} can be assigned to the vibrational coherences in the B state of iodine around $v' \approx 7$, while the peak at 208 cm^{-1} corresponds to the second overtone ($\Delta v'' = 3$) of iodine in the electronic ground state. That is exactly what could be expected from the experimental conditions as mentioned above.

DFWM where all laser pulses possess the same frequency making them indistinguishable in their temporal sequence, apart from their phase conjugation is the most general form of the FWM. By introducing different color schemes into the FWM process, the pulses become differentiable, allowing for the variation of their temporal sequence in the FWM process. This makes the selective preparation and probing of different molecular states possible. Of particular interest is the temporal sequence of the laser pulses that was classified as positive

delay times ($\Delta t > 0$) since the preparation of a molecular state by the a pulse pair (k_1; k_2) brings the influence of a Raman resonance into the selectivity of the states prepared by the respective FWM process. The consideration of Raman resonances in the multi-color schemes of CARS and CSRS call for the comparison of schemes that utilize virtual states for the realization of these processes versus schemes that take place in resonance to the molecular states offered by the system.

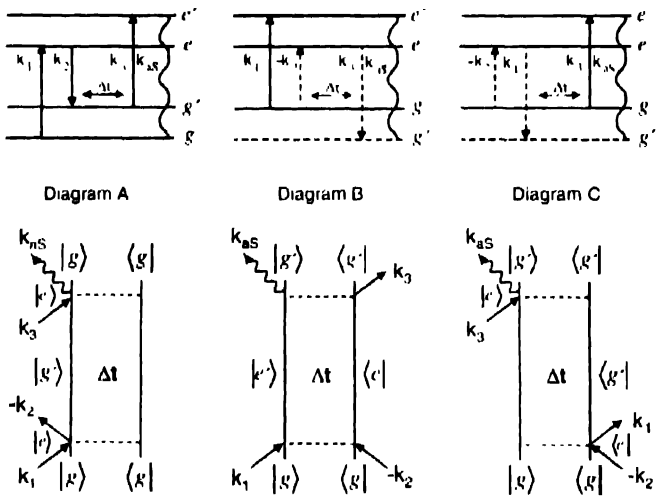

Figure 3. Diagrams *A*-*C* show three possible optical processes in the color scheme of a CARS experiment in a schematic potential energy diagram (top), and double-sided Feynman diagram (bottom) representation. Diagram *A* shows a process that is in full resonance with molecular states (solid horizontal lines), while diagrams *B* and *C* utilize virtual states (dashed horizontal lines).

In Figure 3, the optical processes associated with time-resolved coherent anti-Stokes Raman scattering (CARS) are shown in potential energy diagrams along with the relevant double-sided Feynman diagrams for this FWM process. [33–35, 40, 47–51] For the case that the *pump/Stokes* pulse pair (k_1, k_2) interacts first with the sample ($\Delta t > 0$), three possible Feynman diagrams can be formulated that lead to the formation of a third-order polarization (*A*–*C* in Figure 3). Experimental and theoretical work in the literature and results presented above in Figure 2(B) shows that diagram *A* describes the optical process that primarily contributes to the third-order polarization in the color scheme of CARS while the contribution of the processes described by diagrams *B* and *C* can be neglected. [32–36, 38–42, 51] Briefly, the selection of diagrams that contribute to the CARS signal is founded in the necessity of processes described by diagrams *B* and *C* to utilize virtual states rather than being in full resonance to the quantum states offered by the respective molecular system. The lack of the Raman resonance makes processes of this type ineffective and therefore, they do not contribute significantly to the CARS signal intensity. Diagram *A* shows the preparation and interrogation of a wavepacket in the electronic ground state that is in full resonance to the molecular states of the system in all four optical transitions and will therefore primarily describe the CARS process. Here, the interaction of the *pump* (k_1) and *Stokes* pulse (k_2) projects the initial ensemble $\left|g^{(0)}\right\rangle$ into an excited vibrational state in the electronic ground state $\left|g'^{(2)}(k_1-k_2)\right\rangle$, via the electronically excited state $\left|e^{(1)}(k_1)\right\rangle$. This state develops in time until the second *pump* pulse (k_1) probes this state at a parametric delay time, Δt. The probing of this state is realized by projecting it into a vibrationally excited state in the excited electronic state, $\left|e'^{(3)}(k_1-k_2+k_3)\right\rangle$ and thereby inducing the third-order polarization between this state and $\left|g^{(0)}\right\rangle$ that has developed in time during Δt. As shown in the potential energy diagram describing the CARS process and the Feynman diagram *A* (Figure 3), the third-order polarization is given by the anti-Stokes transition, k_{aS} which is blue shifted relative to the wavelength of the *pump* lasers and described by the transition dipole moment, μ_{aS} :

$$P^{(3)}(\Delta t, k_1-k_2+k_3)=\left\langle g^{(0)}\left|\mu_{aS}\right|e'^{(3)}(k_1-k_2+k_3)\right\rangle+cc. \quad (5)$$

The DFWM transient for $\Delta t > 0$ shows that there is no preference between preparation and interrogation of wavepackets on the electronically excited and ground state potential. Since the utilization of Raman resonances is not possible for DFWM, there is no preference between the formation of ground state versus B-state population gratings, by the interaction of k_2 and k_1. Despite the possibility of Raman resonances in the CSRS process, the transient of this process for $\Delta t > 0$ shown in panel C of Figure 2 shows wavepacket dynamics in the excited B and ground state potential. Figure 4 shows the potential energy diagrams and relevant double-sided Feynman diagrams for time-resolved coherent Stokes Raman Scattering (CSRS). At first, this FWM technique appears very

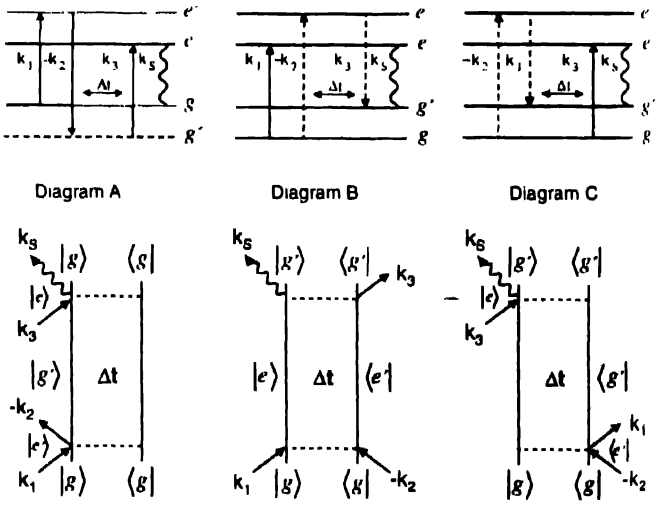

Figure 4. Diagrams *A*-*C* show three possible optical processes in the color scheme of a CSRS experiment in a potential energy diagram (top), and double-sided Feynman diagram (bottom) representation. Diagrams *B* and C show processes that are in full resonance with molecular states (solid horizontal lines), while diagrams *A* utilize virtual states (dashed horizontal lines).

similar to CARS but the process shows a much higher complexity than CARS in its interpretation. For this configuration, the Feynman diagrams ***B*** and ***C*** in Figure 4 show the relevant contributions to the CSRS signal. Here all optical transitions are in resonance to the quantum state of the system, while diagram *A* utilizes virtual states and will therefore not contribute significantly to the CSRS signal [33–35, 40–42, 51] However the contribution of Feynman diagram ***A*** to the CSRS process, showing a scenario that utilizes a virtual state is difficult to evaluate since both potentials are already accessed by the resonant processes given by diagrams ***B*** and ***C***. The latter show the formation and propagation of an excited electronic state, $\left|e'^{(1)}(\boldsymbol{k}_1)\right\rangle$ or $\left|e'^{(1)}(-\boldsymbol{k}_2)\right\rangle$ and an electronic ground state, $\left|g'^{(2)}(-\boldsymbol{k}_1+\boldsymbol{k}_2)\right\rangle$, respectively. Both ground and electronic excited state dynamics will be observed in the transient signal as a function of Δt and must both be considered in the expression for the third-order polarization of the CSRS process. Here, diagram ***B*** is described by the first term in equation (6), where the dynamics of the electronically excited state, $\left|e'^{(1)}(-\boldsymbol{k}_2)\right\rangle$ are interrogated by projecting into $\left|g'^{(2)}(-\boldsymbol{k}_2+\boldsymbol{k}_3)\right\rangle$ with the time variable *pump* laser, $\boldsymbol{k}_3$. Diagram *C* contributes to the second term of equation (6), where the dynamics of the electronic ground state, $g'^{(2)}(-\boldsymbol{k}_2+\boldsymbol{k}_1)\rangle$ are interrogated by projecting $\left|g^{(0)}\right\rangle$ into $\left|e^{(1)}(\boldsymbol{k}_3)\right\rangle$ with the time variable *pump* laser, $\boldsymbol{k}_3$. For both cases, the third-order polarization is given by the *Stokes* transition, which is spectrally red shifted to the wavelength of the *pump* lasers and described by the transition dipole moment for the Stokes transition, μ_S. With similar considerations that were made for the formulation of the CARS signal, the third-order polarization of CSRS process can be developed as follows :

$$P^{(3)}(\Delta t, \boldsymbol{k}_1-\boldsymbol{k}_2+\boldsymbol{k}_3)=\left\{\left\langle g'^{(2)}(\boldsymbol{k}_2-\boldsymbol{k}_3)\middle|\mu\middle|e^{(1)}(\boldsymbol{k}_1)\right\rangle\right.$$
$$\left.+\left\langle g'^{(2)}(\boldsymbol{k}_2-\boldsymbol{k}_1)\middle|\mu\middle|e^{(1)}(\boldsymbol{k}_3)\right\rangle\right\}+cc. \qquad (6)$$

In summary, for the CARS process, the Raman resonance allows for a higher selectivity than in the case of DFWM and CSRS

The femtosecond laser pulses, employed in generating the four-wave mixing signal, possess a spectral bandwidth that exceeds the energy spacing of the vibrational states accessed in molecular iodine. This opens the possibility of generating a variety of multi-color schemes such as CARS and CSRS parallel to the DFWM process, since the necessary wavelengths for these multi-color schemes are included in the bandwidth of the laser pulses. The different FWM processes will show themselves at different spectral positions of the broadband signal and a CCD multichannel detector allows for the dynamics generated by these processes to be characterized simultaneously by the broadband detection of the spectrally dispersed signal. The simultaneous generation and detection of a CARS, CSRS and DFWM process in a time-resolved scheme allows for a direct comparison of the molecular states that are prepared, propagated and interrogated by these processes under identical experimental conditions.

The FWM signal intensity can be plotted as a function of the respective detection wavelength, λ_{det} and the delay time, Δt of the time variable laser pulse $\boldsymbol{k}_3$. A contour plot of this type is shown in Figure 5. The modulations of the intensity along the time axis can be seen across the full spectral width of the recorded FWM signal. In order to obtain a more detailed view of the time domain behavior of the signal, cross-sections of the contour plot along the time axis at a fixed detection wavelength are made. An analysis of the different dynamics observed within the FWM signals with the help of these cross-sections shows that there are three characteristic contributions within the spectral components of the signal pulse.

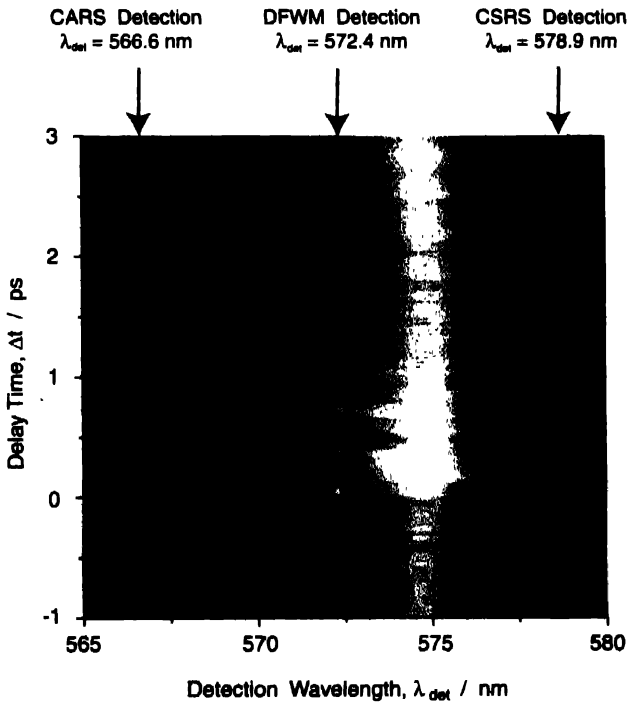

Figure 5. Contour plot of the DFWM intensity as a function of the delay time, Δt and the detection wavelength, λ_{det} acquired by CCD multichannel detection of the DFWM spectrum for varying delay times. Cuts made along the time axis show that the DFWM signal shows dynamics characteristic for DFWM as well as CARS and CSRS processes (See Figure 6).

The spectral position of these three distinct contributions are marked in Figure 5 and the dynamics are plotted in panels *A–C* in Figure 6 for the central wavelength of the pulse (λ_{det} = 572.4 nm), blue shifted from the central wavelength (λ_{det} = 566.6 nm) and another shifted to the red flank of the pulse (λ_{det} =578.9 nm). Generally, this change in the behavior of the signal with

respect to the detection wavelength can be attributed to the polychromatic nature of the broadband fs laser pulses employed in the experiment. The different wavelengths incorporated in the spectral profile of the laser pulses allow for three different FWM processes, CARS, DFWM and CSRS, to be generated simultaneously in the sample. The identification of the three FWM processes at different wavelengths of the broadband signal can be made when the characteristic state selectivity, that manifests itself in the preparation of vibrational wavepackets on different electronic potentials of the molecular system, is compared to experiments presented in Figure 2(A)-(C), where these three FWM processes are explicitly carried out on gaseous iodine [33–35, 40–42, 51].

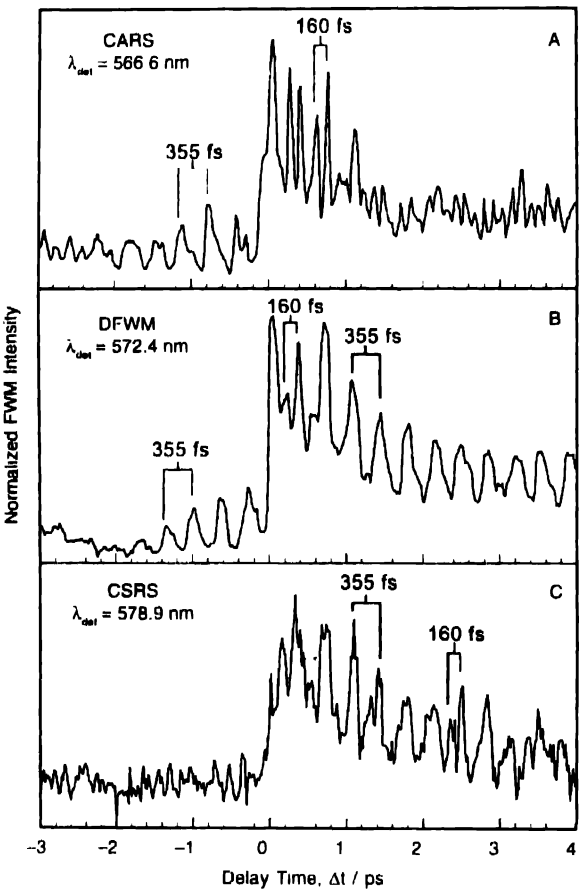

Figure 6. Diagrams A-C show three cross-sections made along the time axis of the contour plot in Figure 5 *A*. At λ_{det} = 566.6 nm, the dynamics reflect the state selectivity of a CARS process *B*. At a detection wavelength of λ_{det} = 572.4 nm, the observed dynamics are representative of a DFWM process C. A shift to the red side of the FWM spectrum shows dynamics of a CSRS process at λ_{det} = 578.9 nm

The detection at the central wavelength of the signal, λ_{det} = 572.4 nm corresponds to a classical DFWM experiment, where the detection wavelength is equivalent to the central wavelength of the three laser pulses. The transient signal at this detection wavelength is shown in panel B of Figure 6. For negative delay times ($\Delta t < 0$), the development of a first-order polarization prepared by k_3 can be observed. This first-order polarization is modulated by a vibrational wavepacket with a period of 355 fs, which corresponds to the vibrational period in the excited B-state of iodine. This assignment is confirmed by the Fourier transformation of the transient for $\Delta t < 0$ in panel C of Figure 7. Here, the two peaks at 92 and 185 cm^{-1}, give the energy spacing between two neighboring vibrational eigenstates ($\Delta v' = 1$) and the first overtone ($\Delta v' = 2$) accessed in the excited B state by a laser pulse with λ = 573 nm. [52, 53] For positive delay times ($\Delta t > 0$), the transient shows the dynamics prepared by the pulse pair (k_1; k_2). Here the superposition of oscillations can be seen that possess a period of approximately 160 fs, corresponding to the period of a vibrational wavepacket in the electronic ground state of iodine around $v'' \approx 0$, and oscillations of 355 fs showing dynamics that can be attributed to the excited B-state. Again, this assignment can be confirmed by the Fourier transformation in panel D of Figure 7, which shows a peak at 211 cm^{-1}, corresponding to the energy spacing of the vibrational eigenstates in the ground state around the vibrational quantum number $v'' = 1$. [54] The two peaks at 93 and 185 cm^{-1} are representative of the excited B state as described above. These findings correspond to the state selectivity expected of the DFWM process shown in Figure 1(A) [33–35, 38–42, 51].

The transient behavior in the blue flank of the FWM signal at λ_{det} = 566.6 nm is shown in panel A of Figure 6. Here, different dynamics are observed in comparison to the transient at λ_{det} = 572.4 nm. With a comparison to CARS experiments on gaseous iodine presented in Figure 1(B), the dynamics observed at this detection wavelength can be attributed to the superposition of a CARS and DFWM process [33–35,38–42,51]. In the case of the CARS process, a wavelength near the maximum of the spectral profile of k_1 will act as a *pump* laser while the spectral region in the red flank of k_2 serves as a *Stokes* laser. The time variable laser, k_3 acts as the second *pump* laser and the coherent anti-Stokes signal is generated in the blue flank of the signal. The oscillations at $\Delta t < 0$ with a period of approximately 355 fs are the result of a first-order polarization modulated by the vibrational wavepacket dynamics of the excited *B*-state. This is confirmed by the appropriate peaks in the Fourier transformation at 94 and 185 cm^{-1} shown in panel A of Figure 7. For $\Delta t > 0$, the transient and the Fourier transformation show a much stronger contribution of the electronic ground state dynamics than the DFWM transient recorded at λ_{det} = 572:4 nm, with oscillations of 160 fs and a corresponding peak in the Fourier transformation in panel B in Figure 7 at 211 cm^{-1}. This rising contribution of the ground state dynamics is attributed to the growing contribution of a CARS process. This will be discussed in greater detail below. Furthermore, the Fourier transformation shows two peaks at 93 and 185 cm^{-1} which cannot be attributed to a CARS process. These peaks are designated to a DFWM process driven by the blue flanks of the laser pulses, and reflect the dynamics of the excited *B*-state. The components at 27, 124 and 280 cm^{-1} can roughly be assigned to the sum and difference wavenumbers

between the wavenumber components of the CARS process at 211 cm^{-1} and the components of the DFWM process at 93 and 185 cm^{-1}. A detection wavelength located on the red side of the signal at λ_{det} = 578.9 nm also shows dynamics different than observed at the central wavelength of the signal. Here, the behavior of the transient signal, displayed in panel C of Figure 6, shows the state selectivity that is characteristic of a coherent Stokes Raman scattering process (CSRS). For the CSRS process, a wavelength near the maximum of the spectral profile of $\hbar k$ will act as a *pump* laser while the spectral region in the blue flank of k serves as an *anti-Stokes* laser. The time variable laser, k_3 acts as the second *pump* laser and the coherent Stokes signal is generated in the red flank of the signal. For $\Delta t < 0$, the transient and the corresponding Fourier transformation show that virtually no dynamics are present for these delay times. This feature is characteristic of a CSRS process observed in Figure 1(C) [33–35, 38–42, 51]. At positive delay times, $\Delta t > 0$ a superposition of ground state and excited B-state dynamics can be observed with oscillations possessing a period of approximately 160 and 355 fs, respectively. The Fourier transformation shows a peak at 94 cm^{-1} which is representative of the excited-*B* state and a weak band in the region from 185 to 215 cm^{-1} poorly resolves the contributions that are expected of the excited B state at approximately 185 cm^{-1} and of the ground state at about 211 cm^{-1}. This is the state selectivity expected for a Raman resonant CSRS process as shown in Figure 1(C). [33–35, 38–42, 51]. The contribution of a DFWM process, driven by the red flank of the laser pulses superimposed on the CSRS process cannot be ruled out since both schemes possess the same state-selectivity for this temporal sequence of the laser pulses. The analysis of the broadband signal with the help of a CCD multichannel detection above shows the possibility of characterizing the time-domain behavior of the different spectral channels of an FWM processes. The comparison of the characteristic time-domain behavior at the specific spectral positions in the DFWM signal with the experiments presented in Figure 2, where CARS, CSRS and DFWM were explicitly carried out on gaseous iodine, allows for an identification of CARS and CSRS processes in the blue and red flank of the DFWM spectrum.

As described above the consideration of Raman resonances in the multi-color schemes of CARS and CSRS call for the comparison of schemes that utilize virtual states for the realization of these processes versus schemes that take place in resonance to the molecular states offered by the system [32–42,48,49,51]. For the CARS process, the Raman resonance allows for a higher selectivity than in the case of DFWM or CSRS. The Feynman diagrams *A–C* in Figure 3 describe the three possible scenarios

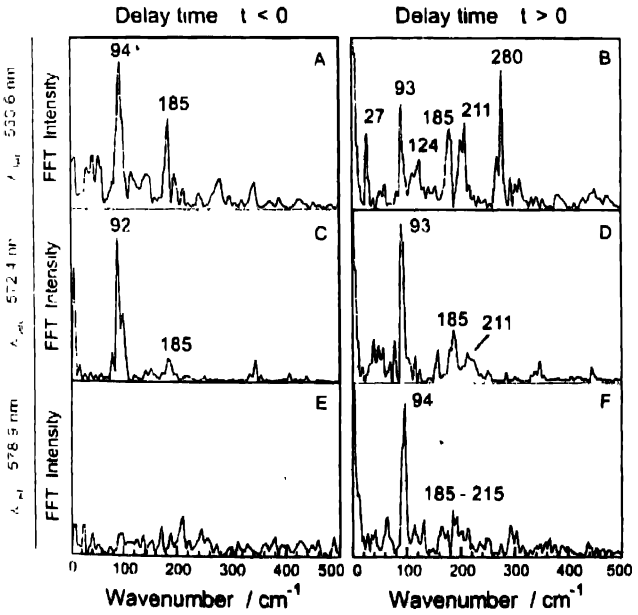

Figure 7. Fourier transformations of the transients in Figure 6. Spectra *A* and *B* show the Fourier transformation for the CARS detection wavelength λ_{det} = 566.6 nm for the two possible temporal sequences of the laser pulses $\Delta t < 0$ and $\Delta t > 0$, respectively. Spectra *C* and *D* show the Fourier transformations for the DFWM detection wavelength at λ_{det} = 572.4 nm and spectra *E* and *F* for the CSRS detection wavelength at λ_{det} = 578.9 nm at the respective delay times.

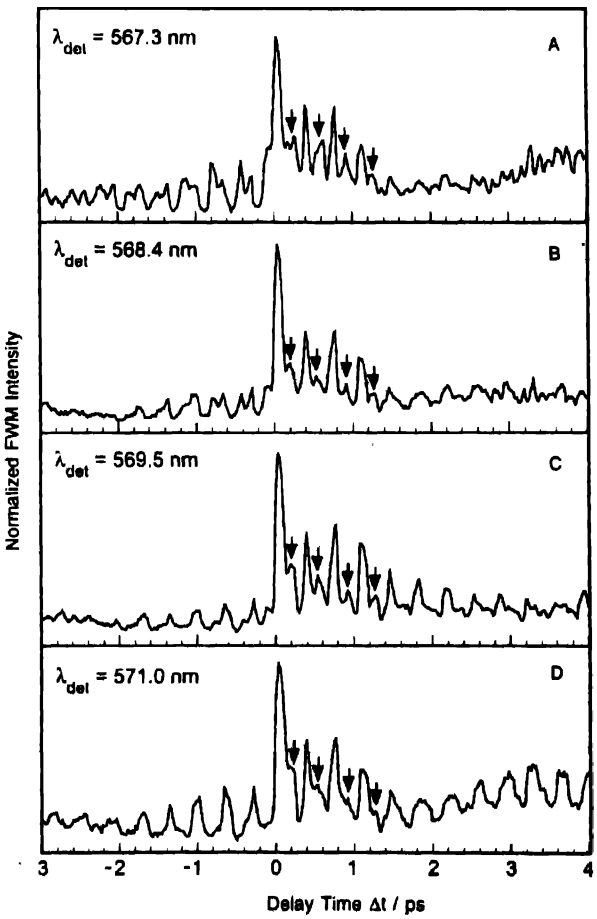

Figure 8. Diagrams *A-D* show four cross-sections made along the time axis of the contour plot in Figure 5. The cross-sections illustrate the growing contribution of ground state dynamics as the detection is shifted from the central wavelength at λ_{det} = 572.4 nm to the blue flank of the FWM signal. Arrows mark the oscillations that are exclusively the result of a wave packet in the electronic ground state of iodine.

for the color scheme of the CARS process for $\Delta t > 0$. While diagrams **B** and **C** show the necessity to utilize a virtual state, diagram **A** shows the preparation and interrogation of a wavepacket in the electronic ground state in full resonance to the quantum states of the molecular system. The relevance of the Raman resonant process described by diagram **A** can be seen in the transient for the CARS detection at λ_{det} = 566:6 nm in Figure 6. Here, the strongest ground state contribution of all detection wavelengths can be seen in a vibrational period of 160 fs, characteristic of a wavepacket in the electronic ground state . This is also evident in Figure 8, where the continuous change in the dynamics, as the detection wavelength is varied from the central wavelength to the blue flank of the signal, shows an increasing ground state contribution. The vibrational period of 160 fs associated with the ground state potential is marked with arrows in the transients of Figure 8, in order to emphasize the growing contribution of the CARS process for the blue-shifted detection wavelengths. The effect of a stronger CARS process can also be seen in the comparison of the Fourier transformations in Figure 7. The amplitude of the band at approximately 210 cm^{-1}, that corresponds to the energy spacing of the vibrational states of the ground state potential, is clearly stronger for the dynamics detected in the blue flank of the signal than at any other detection wavelength. The other bands in the Fourier transformation of the transient detected at λ_{det} = 566.6 nm can be attributed to a DFWM process driven by the blue flanks of the laser pulses at this wavelength and sum and difference frequencies of CARS and DFWM processes. The possibility that these excited state dynamics are the result of a CARS process can be ruled out by comparisons with Figure 2(B), where a CARS process on gaseous iodine only shows dynamics in the electronic ground state for $\Delta t > 0$.

In summary, the generation of the coherent Raman processes of CARS and CSRS parallel to the DFWM process, allows for a direct comparison of these FWM schemes. This is valuable for the analysis of the state-selectivity, that presents itself in the preparation of vibrational wavepackets on different electronic potentials of the molecular system. The selectivity of CARS dominated by the process described by Feynman diagram **A** in Figure 3 is the most significant result of the experiments presented above. This dominant contribution of a single Feynman diagram to the CARS process, shows the significance of Raman resonance in comparison to processes that utilize virtual states. The concept, that Raman resonances lead to relevant contributions to the signal intensity of a FWM process while processes utilizing virtual states will not, was addressed in this chapter in the simple molecular system of gaseous iodine.

4.2 Spectrally dispersed femtosecond-CARS of MgOEP :

As shown in the previous subsection, vibrational dynamics in the ground state of molecules can be accessed using time-resolved femtosecond CARS spectroscopy. While in diatomic molecules only one vibrational mode is excited, in larger molecules an ensemble of different vibrational motions is involved in a femtosecond experiment. In the following we want to concentrate on a description of fs-CARS considering the special situation where the anti-Stokes signal is recorded, spectrally dispersed by means of a CCD camera, as a function of positive delay times. We will mainly focus on the spectral information (and mode assignment) that can be deduced from such measurements by employing Fourier transform methods to the two-dimensionally recorded transient signal.

In this section, we present spectrally dispersed fs-CARS measurements on magnesiumoctaethyl-porphyrin (MgOEP) [43-45]. In Figure 9, we show the wavelength arrangement of the laser beams together with the absorption spectrum of MgOEP in dichloromethane. The pump pulse (k_1 /k_2) wavelength of 581 nm roughly coincides with the Q_{00} absorption band maximum at 580 nm The Stokes pulse (k_2) is tuned to 632 nm, resulting in an anti-Stokes signal (aS) centered at 538 nm, in the vicinity of the Q_{01} -band maximum

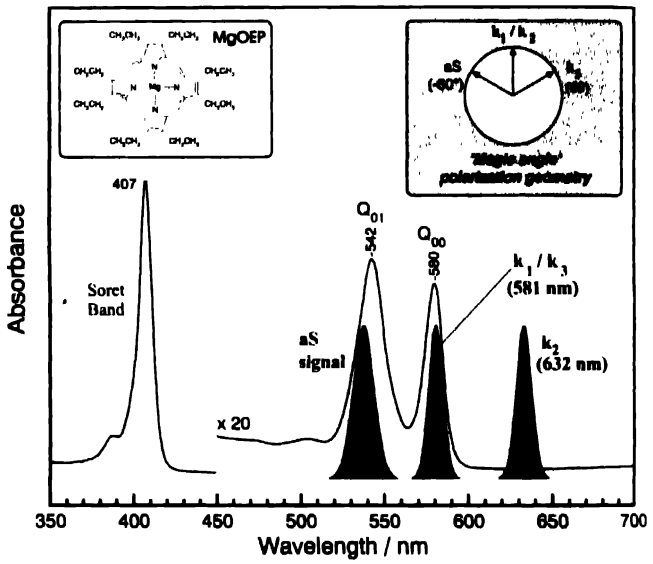

Figure 9. fs-CARS wavelength arrangement and absorption spectrum of MgOEP dissolved in Cl2 CH2

The vibrational information which one wishes to extract from the transient CARS signal is often obscured by non–Raman resonant contributions. This is especially a problem when, like here, the molecular system investigated is studied in solution the decay of the resonant isotropic contribution, which corresponds to pure vibrational dynamics, occurs on a much faster timescale than in isolated molecules and, additionally, the non-resonant CARS signal from the solvent is often orders of magnitude higher than the signal from the system one intends to study. The overall wavelength arrangement leads to a strong resonance enhancement of the CARS process. In order to suppress non-Raman resonant scattering contributions from the solvent to the CARS signal around Δt = 0, a magic angle polarization geometry for the four beams has been applied in

hese measurements [55]. We keep the temporally overlapping ump (k_1) and Stokes (k_2) pulses parallel polarized (0°), and set he time-delayed pump pulse (k_3) and the anti-Stokes signal aS) to – 60° and – 60°, respectively (see inset of Figure 9).

Figure 10(A) shows a typical spectrally dispersed transient CARS signal as a function of the delay time Δt between the ump pulse (k_3) and the two time-coincident pulses k_1 and k_2 nd of the CARS wavenumber $\tilde{\nu}_{aS}$. It has been obtained from MgOEP dissolved in dichloromethane, for a pump pulse wavelength of 580 nm and a Stokes pulse wavelength of 631 nm. The signal is centered at about $\tilde{\nu}_{aS} = 1400\,\mathrm{cm}^{-1}$, corresponding to the mean excitation energy determined by the wavenumber difference of the pump and the Stokes laser. It extends from $\tilde{\nu}_{aS} = 1000\,\mathrm{cm}^{-1}$ to $\tilde{\nu}_{aS} = 1800\,\mathrm{cm}^{-1}$. In the vibrational spectrum of MgOEP this is the interesting region where modes of the porphyrin macro-cycle are predominantly located [56]. The signal lasts for about 4 ps and shows the expected oscillatory pattern for the high density of coherently excited normal modes in the ground state of this system, with a strongly modulated structure in both, the direction of the time axis and the wavenumber axis.

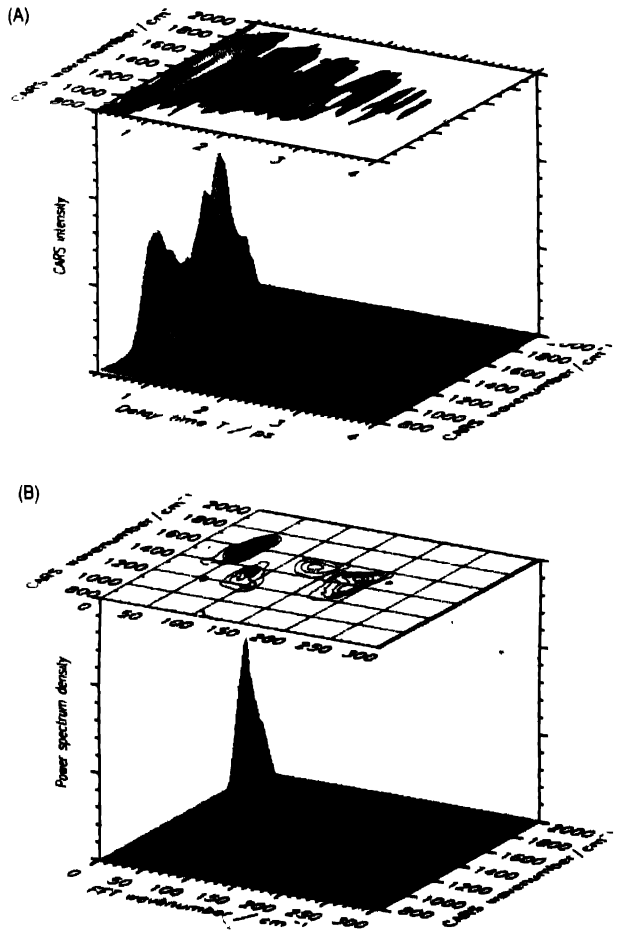

gure 10. (A) Spectrally dispersed transient CARS signal of MgOEP. (B) wer spectrum density (PSD) of the oscillating contributions to the nsient CARS signal of Figure 2(A)

To further investigate the wavenumber spectrum of the oscillatory structure comprised in the signal of Figure 10(A), we have calculated the power spectrum density (PSD) of the time-domain signal with the fast Fourier transform method (FFT), which is shown in Figure 10(B). The PSD elucidates the quantum beat dynamics of the vibrational coherence generated in the wavenumber domain. It is now obvious that the complex oscillatory pattern of the time-domain signal is mainly attributable to four peaks (Table 1). The peak location along the FFT wavenumber axis corresponds to the wavenumber differences of two coherently excited vibrational modes of MgOEP, and the location along the CARS wavenumber axis is approximately given by the arithmetic mean wavenumber position of the two beating modes.

Table 1. FFT wavenumber ($\tilde{\nu}_{FFT}$) and CARS wavenumber ($\tilde{\nu}_{CARS}$) locations of the peaks in the PSD plot (Figure 10(B)). The peaks correspond to quantum beatings between the vibrational modes ν_k and ν_l of MgOEP.

$\tilde{\nu}_{FFT}$ /cm^{-1}	$\tilde{\nu}_{CARS}$ /cm^{-1}	ν_k, $\tilde{\nu}_k$ /cm^{-1}	ν_l, $\tilde{\nu}_l$ /cm^{-1}	$\tilde{\nu}_l - \tilde{\nu}_k$ /cm^{-1}
52	1570	$\nu_{11}(b_{1g})$, 1552	$\nu_{10}(b_{1g})$, 1606	54
84	1330	$\nu_{21}(a_{2g})$, 1317	$\nu_{20}(b_{2g})$, 1400	83
130	1530	$\nu_3(a_{1g})$, 1477	$\nu_{10}(b_{1g})$, 1606	129
182	1475	$\nu_{20}(b_{2g})$, 1400	$\nu_2(a_{1g})$, 1579	179
		$\nu_4(a_{1g})$, 1372	$\nu_{11}(b_{1g})$, 1552	180

It is now appropriate to compare the obtained results with data that are available from spectrally resolved techniques on the same molecule [56]. In order to assign the peaks in the PSD to the wavenumber difference of two vibrational modes ν_k and ν_l, results from ns-CARS spectroscopy and resonance Raman measurements have been taken into account (see Table 1). Because of the well defined polarization directions of the CARS signal contributions from individual vibrational modes, the quantum beat structure of the detected signal is influenced by the magic angle polarization geometry of the laser beams [56]. Contrary to ns-CARS though, where all three incident laser beams are temporally overlapped and fixed, in fs-CARS one is able to analyze the signal at delay times when the non-Raman resonant scattering contribution is already decayed. Therefore, when the pulse duration of the laser pulses is considerably shorter than the vibrational dephasing time, the non-Raman resonant background does not obscure the signal at Δt, leaving the analyzer setting of the CARS signal in principle undetermined.

Using this concept, transient CARS measurements on magnesiumtetraphenylporphyrin (MgTPP) have been performed, where the coherent vibrational motion detected is selected by the polarization direction of the analyzer used for the CARS signal beam. The electronic resonance conditions in these measurements have been the same as for the MgOEP measurements. The mean excitation wavenumber was 1400

cm^{-1}. Panel (A) of Figure 11 shows the PSD of the transient CARS signal for the same magic angle polarization arrangement

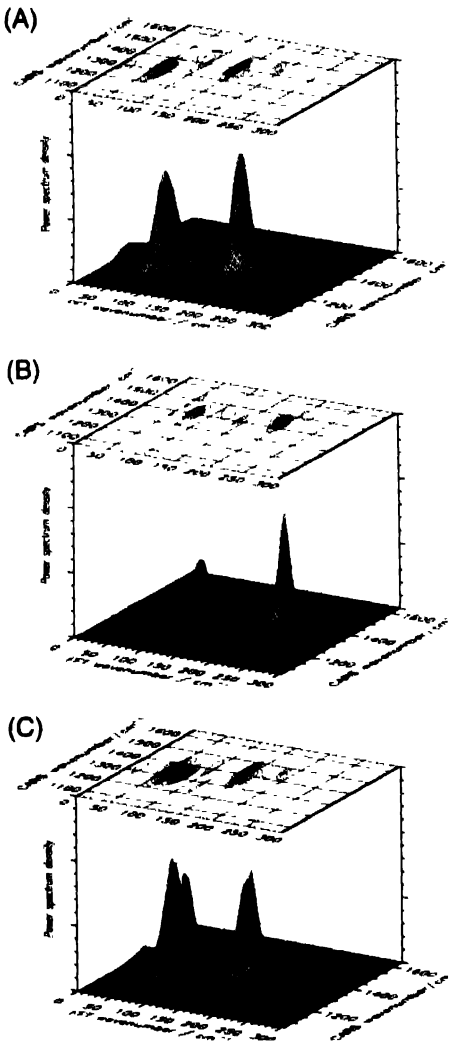

Figure 11. Power spectrum density of the transient CARS signal of MgTPP for three different polarization geometries: (A) CARS signal analyzer setting -60±, (B) 0±, (C) -78±

(analyzer polarization -60° with respect to the pump/Stokes polarizations) as in the measurements on MgOEP. Four peaks are observable in the resulting signal. The assignment of the contributing modes and their respective symmetries are given in Table 2. Almost no cw data are available for the MgTPP system because of the strong fluorescence background in resonance Raman spectra (Q-band excitation). Therefore, the assignment is mainly based on results on NiTPP [57].

Table 2. Mode assignment to the PSD peaks of the polarization sensitive fs-CARS measurements on MgTPP (Figure 11)

ν_{FFT} /cm	ν_{CARS} /cm	$\nu_k, \tilde{\nu}_k$ /cm	$\nu_l, \tilde{\nu}_l$ /cm	$\tilde{\nu}_l - \tilde{\nu}_k$ /cm
62	1310	$\nu_{27}(b_{2g})$ 1249	$\nu_{30}(a_{2g})$ 1321	≈ 72
88	1420	$\nu_{29}(b_{2g})$ 1357	$\nu_{28}(b_{2g})$ 1465	≈ 108
142	1410	$\nu_{30}(a_{2g})$ 1321	$\nu_{28}(b_{2g})$ 1465	≈ 144
192	1435	$\nu_{32}(b_{1g})$ 1282	$\nu_{31}(b_{1g})$ 1496	≈ 214

Assuming that the depolarization ratios for conventional CARS are valid for the measurements presented here, the contribution to the signal should vanish for an analyzer setting of 0° for modes of a_{2g} symmetry, and at -78° for modes of b_{1g} and b_{2g} symmetry. Panel (B) of Figure 11 shows the PSD of the transient signal for an analyzer setting of 0°. The peak structure is basically the same as in the magic angle measurement. However, the intensity of the peak originating from two b_{1g} modes has strongly increased, whereas the two peaks from a a_{2g} mode have considerably decreased in relative intensity. The PSD shown in panel (C) of Figure 11, depicting the measurement at an analyzer setting of -78°, is similar to the one given in panel (A). The peaks from modes with a_{2g} symmetry are now clearly dominating. All features containing contributions from b_{1g} and b_{2g} modes are now even further suppressed. The results presented for the three different polarization geometries are in accordance with the expectation that the dynamics detected depend strongly on the polarization geometry employed. The tentative mode assignment in Table 2, from NiTPP data, is confirmed.

5. Conclusion

In this paper, we have reviewed work on femtosecond time resolved FWM spectroscopy performed in our laboratories. We concentrated mainly on experimental details and partially on their interpretation.

First we have demonstrated how the many degrees of freedom offered by the FWM techniques, can be used to gain information about molecular wavepacket dynamics evolving on different PESs. These experiments were performed on iodine in the gas phase which serves as a simple model system. For the FWM process three laser pulses interact with the molecules generating a nonlinear response signal. The following parameters had been varied: (i) the timing of the laser pulses — using femtosecond laser pulses, we were able to coherently excite and probe wavepackets. By changing the sequence of the laser pulses, dynamics on different PESs contribute to the FWM signal. A separation of excited–state and ground–state vibratonal coherences is possible; (ii) the laser wavelength — electronic as well as ro-vibratioal resonances and through this the energy position where the wavepackets are prepared on the PES of the molecules depend on the laser wavelengths; (iv) the wavelength window which is opened for the detection of the FWM signal — we showed that this parameter is very important as it selects different dynamics contained in the transients. By using a multichannel detection technique (three –dimensional) transients can be taken which give the FWM intensity as a function of delay time between the laser pulses and wavelength of the FWM signal.

After discussing the possibilities of the femtosecond time-resolved FWM technique, we introduced a more specific experiment on a more complex molecular system. Here, we demonstrate that FWM is a very useful method for exciting and probing molecular dynamics in the ground state. We applied femtosecond time-resolved CARS spectroscopy to large polyatomic porphyrin systems. By employing spectrally dispersed fs-CARS we have excited and probed coherent vibrational motion in the electronic ground state of these systems. We have demonstrated that the method is able to provide a detailed mapping of the dynamics of a multitude of excited modes and that it yields the dephasing behaviour and spectral information at the same time. We have shown that the vibrational dynamics detected can be efficiently selected by varying the polarization direction of the CARS signal analyzer. The results presented demonstrate that CARS spectroscopy with femtosecond time resolution and wavenumber-resolved detection is a powerful tool not only for the characterization of dynamics in the electronic ground state but also for the selective generation and detection of the different vibrational motions of large molecules.

Acknowledgements

This work was funded by the Deutsche Forschungsgemeinschaft (Schwerpunktprogramm "Femto-sekunden-Spektroskopie elementarer Anregungen in Atomen, Molekülen und Cluster," Projekt KI 202/14-2; SFB 347 Projekt C2). We also acknowledge financial support from the Fonds der Chemischen Industrie. Stimulating discussions with Prof. Dr. Volker Engel and Prof. Dr. Arnulf Materny are gratefully acknowledged.

References

[1] C V Raman and K S Krishnan *Nature* **121** 501 (1928)

[2] P D Maker and R W Terhune *Phys. Rev.* **A137** 801 (1965)

[3] R Leonhardt, W Holzapfel, W Zinth and W Kaiser *Chem. Phys. Lett.* **133** 373 (1987)

[4] W Zinth, R Leonhardt, W Holzapfel and W Kaiser *IEEE J. Quant. Electron.* **24** 455 (1988)

[5] T Lang, K-L Kompa and M Motzkus *Chem. Phys. Lett.* **310** 65 (1999)

[6] W E Bron, T Juhasz and S Mehta *Phys. Rev. Lett.* **62** 1655 (1989)

[7] H Okamoto and K Yoshihara *J. Opt. Soc. Am.* **B 7** 1702 (1990)

[8] H Okamoto and K Yoshihara *Chem. Phys. Lett.* **177** 568 (1991)

[9] T Joo, M A Dugan and A C Albrecht *Chem. Phys. Lett.* **177** 4 (1991)

[10] M Fickenscher, H-G Purucker and A Laubereau *Chem. Phys. Lett.* **191** 182 (1992)

[11] H Okamoto, R Inaba, K Yoshihara and M Tasumi *Chem. Phys. Lett.* **202** 161 (1993)

[12] T-S Yang, R Zhang and A B Myers *J. Chem. Phys.* **100** 8573 (1994)

[13] C C Hayden, D W Chandler *J. Chem. Phys.* **103** 10465 (1995)

[14] E J Heller *Acc. Chem. Res.* **14** 368 (1981)

[15] E J Heller and R L Sundberg *J. Phys. Chem.* **86** 1882 (1982)

[16] S Mukamel and R F Loring *J. Opt. Soc. Am. B* **3** 595 (1986)

[17] V F Kamalov and Y P Svirko *Chem. Phys. Lett.* 194 13 (1992)

[18] A Laubereau and W Kaiser *Rev. Mod. Phys.* 50 607 (1978)

[19] I. I. Abram, R M Hochstrasser, J E Kohl, M G Semack and D White *J. Chem. Phys.* **71** 153 (1979)

[20] B H Hesp and D A Wiersma *Chem. Phys. Lett.* **75** 423 (1980)

[21] D D Dlott, C L Schlosser and E L Chronister *Chem. Phys. Lett.* **30** 986 (1982)

[22] F Ho, W S Tsay, J Trout, and R M Hochstrasser *Chem. Phys. Lett.* **83** 5 (1981)

[23] W Zinth, R Leonhardt, W Holzapfel and W Kaiser *IEEE J. Quant. Electron* **QE-24**, 455 (1988)

[24] R Inaba, H Okamoto, K Yoshihara and M Tasumi *Chem. Phys. Lett.* **185** 56 (1991)

[25] H-G Purucker, V Tunkin and A Laubereau *J. Raman Spectrosc.* **24** 453 (1993)

[26] T Joo and A C Albrecht *Chem. Phys.* **176** 233 (1993)

[27] M Motzkus, S Pedersen and A H Zewail *J. Phys. Chem.* **100** 5620 (1996)

[28] J A Shirley, R J Hall and A C Eckbreth *Opt. Lett.* **5** 380 (1980)

[29] Y Prior *Appl. Opt.* **19** 1741 (1980)

[30] S Maeda, T Kamisuki and Y Adachi in *Advances in Non-Linear (Chichester : Spectroscopy*, R J H Clark, R E Hester, (Eds) John Wiley & Sons) (1988)

[31] M A Buntine, D W Chandler and C C Hayden *J. Chem. Phys.* **97**, 707 (1992)

[32] M Schmitt, G Knopp, A Materny and W Kiefer *Chem. Phys. Lett.* **270** 9 (1997)

[33] M Schmitt, G Knopp, A Materny and W Kiefer *Chem. Phys. Lett.* **280** 339 (1997)

[34] S Meyer, M Schmitt, A Materny, W Kiefer and V Engel *Chem. Phys. Lett.* **281** 332 (1997)

[35] S Meyer, M Schmitt, A Materny, W Kiefer and V Engel, *Chem. Phys. Lett* **301** 248 (1999)

[36] M Schmitt, G Knopp, A Materny and W Kiefer *J. Phys. Chem.* **A 102** 4059 (1998)

[37] O Rubner, M Schmitt, G Knopp, A Materny, W Kiefer and V Engel *J. Phys. Chem.* **A102** 9734 (1998)

[38] T Chen, V Engel, M Heid, W Kiefer, G Knopp, A Materny, S Meyer, R Pausch, M Schmitt, H Schwoerer and T Siebert *Vib. Spectrosc.* **19** 23 (1999)

[39] T Chen, H Dietz, V Engel, M Heid, W Kiefer, G Knopp, A Materny, S Meyer, R Pausch, M Schmitt, H Schwoerer and T Siebert *SPIE Proc.* **3733** 2 (1999)

[40] T Chen, V Engel, M Heid, W Kiefer, G Knopp, A Materny, S Meyer, R Pausch, M Schmitt, H Schwoerer and T Siebert *J. Mol. Struct.* **480-481** 33 (1999)

[41] T Siebert, M Schmitt, T Michelis, A Materny and W Kiefer *J. Raman Spectrosc.* **30**, 807 (1999)

[42] T Siebert, M Schmitt, A Vierheilig, G Flachenecker, A Materny, and W Kiefer, *J. Raman Spectrosc.* **31** 25 (2000)

[43] M Heid, T Chen, U Schmitt and W Kiefer *Chem. Phys. Lett.* **334** 119 (2001)

[44] M Heid, S Schlücker, U Schmitt and T Chen, R Schweitzer-Stenner, V Engel and W Kiefer *J Raman Spectrosc.* **32**, 771 (2001)

[45] M Heid, T Chen, A Materny and W Kiefer In *Proceedings of the International Conf on Lasers'98*, V J Corcoran, T A Goldman, (Eds) STS Press McLean, 181 (2001)

[46] W Kiefer and H J Bernstein *J Mol Spectrosc* **43** 366 (1972)

[47] S A J Druet and J-P E Taran *Progr Quant Electr* **7** 1 (1981)

[48] D Lee, A C Albrecht, In *Advances in Infrared and Raman Spectroscopy*, R J H Clark, R E Hester (Eds), Vol 12, (John Wiley & Sons), (1985) page 179

[49] D Lee and A C Albrecht In *Adv Chem Phys* , I Prigogine, S A Rice, (Eds), Vol. 83; J Wiley & Sons Chichester, (1993) page 43

[50] A Materny, T Siebert, M Schmitt, G Knopp and W Kiefer In *Proceedings of the International Conference on Lasers'98*, V J Corcoran, T A Goldman, (Eds), STS Press McLean, (1999) p 57

[51] S Meyer and V Engel *J Raman Spectrosc* **31** 33 (2000)

[52] W Kiefer, H J Bernstein, H Wieser and M Danyluk *J Molec Spectrosc* **43** 393 (1972)

[53] J A Coxon, *J Quant Spectrosc Radiat Transfer* **11** 443 (1971)

[54] J Tellinghuisen *J Chem Phys* **58** 2821 (1973)

[55] W Li, H-G Purucker and A Laubereau, *Opt Commun.* **94** 300 (1992)

[56] M Nissum, M J Funk and W Kiefer *J Raman Spectrosc* **30** 605 (1999)

[57] Y S Li and K R Wilson *J Chem Phys* **93** 8821 (1990)

About the Author

WOLFGANG KIEFER was educated at the University of Munich in Germany receiving both his Diploma in Physics in 1967 and his Ph.D. in Physics in 1970 from that institution. From 1970-1972, Dr. Kiefer served as a Postdoctorate Fellow at the National Research Council of Canada in the Division of Chemistry. From there he went to the University of Munich as Assistant in the Department of Physics. In 1977, Dr. Kiefer left the University of Munich to become Professor for Experimental Physics at the university of Bayreuth in Germany followed by Full Professor/head of the Institute for Experimental Physics at the University of Graz in Austria. In 1988, he took a position as Full Professor for Physical Chemistry at the University of Würzburg in Germany. From 1996-1997 he served as Vice Dean of Faculty of Chemistry and Pharmacy at the University and from 1997-1999 as Dean of Faculty of Chemistry and Pharmacy.

Dr. Kiefer has been involved in numerous national and international activities over the course of his career. These include European Editor (Molecular Spectroscopy) for the journal, *Applied Spectroscopy*, member of the Editorial board, Associate Editor and Editor-in-Chief of the *Journal of Raman Spectroscopy*, Member of the Editorial Boards of the *Asian Journal of Physics*, *Spectroscopy Letters*, *Trends in Applied Spectroscopy*, *Asian Chemistry Letters*, and *Chemical Physics Letters*. He has been a member of the IUPAC Commission for Infrared and Raman Spectroscopy, Director of a NATO Institute on Nonlinear Raman Spectroscopy, an Association of British Spectroscopy, Director of a NATO Institute on Nonlinear Raman Spectroscopy, an Association of British Spectroscopists Lecturer, and a member of several Steering Committees. Dr. Kiefer was Chairman of the XIII International Conference on Raman Spectroscopy and he served as Chairman of the International Steering Committee for International Raman Conferences. He was Visiting Professor of Hong Kong University of Science and Technology, Waseda University, Tokyo, Zhengzhou University, P. R. China and he is Honorary Professor of Wuhan University, P. R. China. Dr. Kiefer is also Honorary Member of the Advisory Board of the committee on Light Scattering of the Chinese Physical Society, Honorary Fellow of the Laser and Spectroscopy Society of India (F L. S. S.) and presently Foreign Councillor of the Institute for Molecular Science, Okazaki National Research Institutes, Japan. He is co-editor of five books and has published more than 600 papers. In 2000 he received the distinguished service award from the Society of Applied Spectroscopy.